Priority Based Critical Load Selection Algorithm for Grid Integrated PV Powered EV Charging System with Optimal DC Link Control

Masiha Aijaz[1,*], Ikhlaq Hussain[2] and Shameem Ahmad Lone[1]

[1]*Department of Electrical Engineering, National Institute of Technology Srinagar, Jammu and Kashmir, India*
[2]*Department of Electrical Engineering, University of Kashmir, Jammu and Kashmir, India*
E-mail: masihaaijaz@gmail.com
[*]*Corresponding Author*

Received 24 September 2021; Accepted 01 April 2022;
Publication 09 December 2022

Abstract

This article presents a single phase double stage photovoltaic (PV) array powered grid connected residential premise integrated with electric vehicle (EV) charging functionality. Taking criticality of the loads into consideration, a unique multi-modal control is developed which ensures incessant power supply to the loads via EVs in case of common occurrences of power interruption thereby enhancing the power security of the system. Favourable regulation of DC link voltage is achieved via proportional integral (PI) controller (DCVPI). Comparison between genetic algorithm (GA) and modified particle swarm optimisation (PSO) based tuning proves modified PSO tuned DCVPI achieves faster convergence and better fitness function evaluation. The system is subjected to various dynamic conditions during which modified PSO tuned DCVPI stabilises to the reference voltage faster and results in 1.38% reduction in overshoots opposed to the manual tuning. The proposed

Distributed Generation & Alternative Energy Journal, Vol. 38_1, 293–318.
doi: 10.13052/dgaej2156-3306.38113

system is designed to work both in grid connected mode as well as islanded mode of operation. Moreover, a resynchronisation control is developed to achieve a seamless transition from islanded mode to grid connected mode post the mitigation of power failure. The proposed system achieves unity power factor and complies with the IEEE -519 power quality standard

Keywords: Power electronics, power quality, photovoltaic (PV), electric vehicle (EV), islanding and resynchronization, optimisation.

1 Introduction

Economically feasible electrification has provided impetus for homeowners to incorporate renewable energy resources (RER) to meet their energy demands. Amongst various RER, solar photovoltaic (PV) array installations lead the race due to winning combination of inexhaustible nature of solar energy, negligible maintenance costs, immobile setup, etc. [1]. Several financial inducements introduced by governments further act as a catalyst to increase the PV penetration into the residential market [2]. The widespread penetration of PV array installations is in alignment with the vision of a decarbonised future. The perception of carbon neutrality is further pushed by aggressive promotion of electrified transport. Electric Vehicles (EV) are being increasingly adopted world over to help in reduction of carbon footprint [3]. Various governments have launched a formidable plan to supplant internal combustion engine (ICE) vehicles with EVs by 2030s [4]. The green virtue of EVs only comes to picture, when they are powered by RER [5]. Thus, PV integration with aforementioned benefits is most suitable for EV charging. Yan et al. in [6] developed a multi stage optimisation algorithm for a commercial building integrated EV charging station which is equipped with PV generation and battery energy storage. Chauhan et al. in [7] present PV integrated battery storage for electrification of rural areas. A PV integrated EV charging system provides a raft of benefits like reduction in usage of fossil fuels for EV charging, helps in saving on electric bills and curtail stress on the grid. [8] discusses the use of solar garages which also provide additional benefit of providing shade to the EVs. Wu et al. in [9] proposes decision making model of PV assisted EV charging station considering PV data, parking behavior and electricity prices. [10] employs foecasting techniques on PV, load and EV profiles to improve energy balance of home systems.

Solar PV assisted EV charging systems are a challenge to maintain in a weak power grid scenario. A common occurrence observed in weak grids is the power curtailment imposed by the utilities due to excessive load demand on the grid. This impacts the consumers negatively as the loads are being disconnected. As a result, lot of literature focuses on this aspect. [11] presents an optimisation framework for scheduling of home appliances considering time based price variations. [12] discuses a flexible approach for EV charging taking into account the uncertainty of RER, geography of the area and user behaviour. [13] discusses seamless transition control of a three phase system integrated with ultracapacitor, storage battery and PV array. [14] proposes a novel control algorithm to supress frequency, voltage, and current variations in a microgrid while transitioning from grid connected to islanded mode of operation.

The DC bus plays an important role in maintaining the stability of the system. It acts an interface between AC side and the DC side in a double stage grid connected converter and decouples the power exchange between the grid and the PV array. Thus, it is imperative to minimise the variation in the DC link voltage arising due to changes in solar insolation, load variation and grid disturbances like voltage sag and swells [15]. Thus, well designed proportional integral (PI) controllers is of utmost importance. The gains of the PI controllers have a significant impact on the overall performance of the PI controller, and hence the governing quantity. The performance of the system can be further improved with optimal gain tuning of the DC link voltage PI controller (DCVPI). The most popular method for PI tuning are Ziegler-Nichols (Z-N) method. The Z-N method commences with zeroing of the integral gain (K_I) and gradually increasing the proportional gain (K_P) until the system exhibits oscillations. Following which, the integral gain is adjusted as a function of the frequency of the oscillation alluded to earlier. However, this method assumes the knowledge of the frequency response of the plant [16]. Moreover, the manual method of iteratively tuning the PI gains is a time consuming process and the chances of incorrect tuning also increases. The literature also reports the use of fuzzy logic-based algorithm for tuning of gains. [17] employs fuzzy logic PID for power quality improvement. The emergence of fractional calculus has led to development of fractional order PI controllers in which the integrator possesses a non-integer order. [18] showed the fractional order PI optimised by water cycle algorithm (WCA). Ant-Lion optimisation (ALO) [19] is utilised to enhance the performance of dynamic voltage restorer (DVR). [20] implements Manta ray

foraging optimization (MRFO) for grid connected PV system. [21] presents the use of harmony search (HS) algorithm for grid-connected PV systems. However, such algorithms are computationally expensive, often require large number of iterations and lagging speed of convergence.

This article presents a single phase double stage grid connected residential premise integrated with PV array with EV charging functionality. The system is developed in a multifunctional way to perform in grid connected mode as well as stand-alone mode. The seamless supply of power to non-linear residential loads is achieved by utilising the EV battery. However, the frequent power disruptions and prolonged use of battery can accelerate battery ageing. Hence, a priority based critical load selection algorithm is presented. The algorithm supplies power to the loads based on its SOC. Favourable regulation of DC link voltage is achieved via proportional integral (PI) controller (DCVPI). In this article, DCVPI is optimally tuned using modified particle swarm optimisation (PSO). PSO is a computationally efficient and simple to use [22]. The performance of the PSO is enhanced by updation of the weight coefficients of the algorithm. Such weight updation bolsters the performance of the algorithm by performing fast exploration of the local search space and increased social activity of the swarm particles. As a result, the modified PSO provides rapid convergence and reduced computational burden. The DCVPI, thus tuned, is regulated at an optimum value. The bi-directional control (BDC) rejects the second harmonic component due to well-regulated DC link voltage which increases the voltage at point of common coupling (PCC).

2 Proposed System

The proposed residential system is presented in Figure 1. It consists of a single phase utility grid interfaced through a two leg voltage source converter (VSC). The system feeds non-linear household loads at the AC end. A PV array is connected at the DC link via a boost converter for maximum power extraction [23]. The array is designed for 6.6 kW with 3 and 11 panels in parallel and series respectively. The boost converter is switched at 20 kHz. The system is equipped with EV charging functionality by means of a bidirectional DC/DC converter at the DC end. The bidirectional converter is switched at 25 kHz. Grid interruption and reconnection is realised using a synchronising switch (SS), whereas an RC ripple filter and AC inductor L_{ac} are connected for mitigation of voltage and current harmonics respectively. Parameters of the proposed system are provided in appendix.

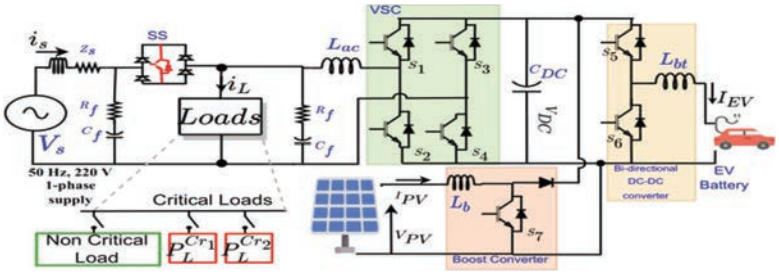

Figure 1 Block diagram of proposed residential nanogrid.

3 Proposed Control

This section describes the various modes of operation of the proposed system. The control strategy adopted in the system is classified on the basis of the controlling quantity and modes of operation. The key sub-control blocks are: maximum power point tracking (MPPT) control, combined DC link and EV battery control, VSC control, grid resynchronisation control and optimal DC link control.

3.1 MPPT Control

In order to maximise the energy harvest of the PV array, the array is always operated at its maximum power point. Vast literature exists to describe various algorithms for MPPT control such as perturb and observe (P&O), fractional open circuit voltage MPPT. Algorithms like fuzzy based approach and neural network based MPPT control [24] are computationally burdensome and require large processing data [25]. In the proposed system, a simple P&O MPPT algorithm is used in conjunction with a boost converter to generate suitable duty cycle to track the MPP for various atmospheric variations as shown in Figure 2.

3.2 Combined DC Link and EV Battery Control

A bi-directional DC/DC converter with two degrees of freedom [1] is used for concurrently controlling the EV current as well as regulation of DC link voltage. Comparison of sensed DC link voltage and prescribed reference voltage is fed to a PI controller which is utilised for regulation of the DC link voltage as given by

$$I_{EVref}(k) = I_{EVref}(k) + k_{vp}(V_e(k) - V_e(k-1)) + k_{vi}V_e(k) \qquad (1)$$

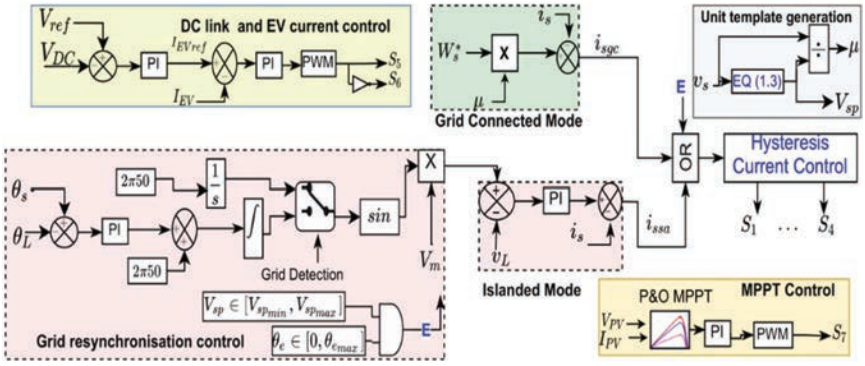

Figure 2 Proposed control diagram.

Where $V_e = V_{ref} - V_{dc}$, k_{vp} and k_{vi} are the gains of the PI controller and I_{EVref} is the generated EV reference current.

Moreover, the resultant error of I_{EVref} and I_{EV} is passed through another PI controller to generate duty cycle for the bi-directional converter. The governing equations for the PI controller as given as

$$d_{EV}(k) = d_{EV}(k) + k_{dp}(I_e(k) - I_e(k-1)) + k_{di}I_e(k) \tag{2}$$

Where $I_e = I_{EVref} - I_{EV}$, k_{dp} and k_{di} are the gains of the PI controller and d_{EV} is the generated duty cycle which is further compared with a repeating sequence to control charging and discharging of the EV battery.

3.3 VSC Control

The VSC control is segmented into two categories on the basis of availability of the grid connection into grid connected mode and islanded mode. The two modes of operation are discussed as follows.

Grid Connected Mode

In this mode, the system under investigation is connected to the grid to deliver power to the loads. The role of EV is to alleviate the burden on the grid by exporting a constant power (P_g^*) to the grid at times of high demand. The governing equations in grid connected mode are as follows.

(a) Unit template generation (μ): The amplitude of the point of common coupling (PCC) voltage is calculated as follows

$$V_{sp} = \sqrt{v_{s1}^2 + v_{s2}^2} \tag{3}$$

Then the in-phase unit template will be calculated as

$$\mu = \frac{v_{s1}}{V_{sp}} \tag{4}$$

Where v_{s1} and v_{s2} are the components of the PCC voltage [26].

(b) Weight of grid power (W_s^*): The weight component of amount of power to be exchanged with the grid, (W_s^*) can be evaluated as follows.

$$W_s^* = \frac{2P^*g}{V_{sp}} \tag{5}$$

Using (3)–(5), the resultant reference current for grid connected mode is generated as shown in Figure 2.

$$i_s^* = Ws^* * \mu \tag{6}$$

The obtained reference current is then compared with the sensed grid current which is then passed to the hysteresis controller, which generates appropriate switching sequence for the VSC.

Islanded Mode and Resynchronisation Control

During any grid disturbance in terms of voltage or frequency, the system must be disconnected from the utility. In the presented system, an islanding algorithm is implemented to detect the non-conformity of standards, following which the proposed system is operated in islanded mode. The phase angles of the grid (θ_{s}) and load voltage (θ_{L}) are compared. The resultant deviation is then passed to the PI controller. The controller equations are as follows

$$\Delta\omega = K_p + (K_i)/(s)(\Delta\theta_s - \theta_L) \tag{7}$$

Where $\Delta\omega$ is the frequency deviation. K_p and K_i are the proportional and integral gains respectively.

Load voltage v_L is compared with the reference voltage generated independently as $V_m sin\omega t$ using 50 Hz as the frequency, where $V_m = 220\sqrt{2}$. Following which, switching pulses are produced by the hysteresis controller as shown in Figure 2.

Once the grid failure is mitigated, the system needs to be resynchronised to the grid. The resynchronisation control is activated which provides a seamless control switch from the islanded mode to the grid connected mode.

A double step check on the phase difference between load phase angle (θ_L) and grid phase angle (θ_s) and the magnitude of grid voltage is performed. The synchronising switch (SS) is turned on following the enabling signal (E) activation once both the checks have been passed and the system is brought on the grid again.

3.4 Priority Based Critical Load Selection Algorithm

A common occurrence observed in weak power grids is the power curtailment imposed by the utilities due to excessive load demand on the grid. During the daylight hours, the result of such power interruptions can be mitigated by complimenting the PV power and power supplied by the EV battery. However, drastic conditions are often presented during the late evening and night hours when the demand of the consumers is peaked. In such a case, the PV generation capability is either entirely absent or insufficient and thus, EV battery operates in vehicle to home (V2H) mode to provide seamless power to the house loads. However, extended use of EV batteries to supply power can result in battery ageing, deterioration thereby shortening its lifespan. Thus, a priority based critical load selection algorithm is presented in the following section. A flowchart depicting the critical load is presented in Figure 3. The residential loads, P_L are categorised as critical and non-critical loads. Moreover, the critical loads are further segregated and denoted eponymously as P_L^{Cr1} and P_L^{Cr2} on the basis of their priority. Following a power interruption, all the non-critical loads are disconnected instantly. The state of charge (SOC) of EV battery acts a reference in the proposed priority load control algorithm. If the SOC is greater than 80%, then both the categories of critical loads remain connected while the EV battery acts in V2H mode. For the SOC range between 60% to 80%, P_L^{Cr1} remains connected while P_L^{Cr2} is turned off. The V2H mode is stopped in entirety for SOC value less than 60%.

3.5 Optimal DC Link Control

The manually tuned DCVPI is replaced by modified PSO based tuning for regulation of DC link voltage. PSO mimics the behaviour of flocking birds to reach the optimum solution. An initial population of particles is randomly generated. Individual particle has an associated velocity which is adapted based on the individual best solution encountered so far called p_{best} and the overall best solution discovered by the entire flock called g_{best}.

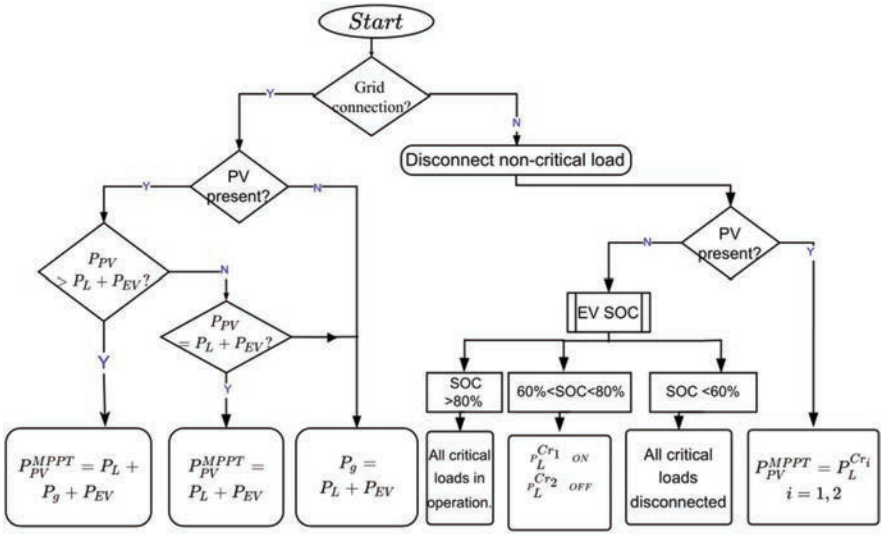

Figure 3 Flowchart depicting priority based load control.

Particle definition

Each individual particle comprises of two DCVPI controller parameters namely k_{pv} and k_{iv}. Thus, the resultant particle K is $K = [k_{pv}, k_{iv}]$. Where k_{pv} and k_{iv} are the proportional and integral gains respectively. The number of particles is (n = 30) and the maximum generations initialised to 30. Bounds on K are depicted as $[l_b u_b] = [00; 2050]$.

Performance criterion

The error generated from voltage reference V_{ref} and DC link voltage V_{dc} serves as the fitness function ϕ as shown in (8).

$$\Phi = \int_0^t (V_{ref} - V_{dc}) \tag{8}$$

In this article, integral time absolute error (ITAE) is chosen as the performance criterion for evaluation of the DCVPI performance. It is depicted in (9).

$$\zeta = \int_0^t t|\Phi|dt \tag{9}$$

Where ζ is the ITAE index.

Updation equations

$$v_{o,q}^{t+1} = w \cdot v_o^t + c_1 * rand_1() * (p_{best_{o,q}} - k_{o,q}^t) + c_2 * rand_2() * (g_{best_{o,q}} - k_{o,q}^t) \quad (10)$$

$$o = 1, 2 \ldots n,$$

$$q = 1, 2$$

$$k_{o,q}^{t+1} = k_{o,q}^t + v_{o,q}^{t+1} \quad (11)$$

From (10), w is the inertia weight factor. c_1, c_2 are acceleration constants. $rand_1()$ and $rand_2()$ are random numbers generated between 0 and 1. The first part of the velocity update equation is referred to as inertia. It represents the tendency of an individual particle to resist any deviation in the direction that it has been travelling. The inertia weight factor is pivotal in governing the stability of the PSO algorithm. The second part models the attraction of the individual particle towards the best position that it has ever found, in other words, personal best solution. The acceleration constant, c_1 is the cognitive coefficient that controls the effect of the individual memory of best solutions. The final component of the updation equation is representative of the migration towards the best position found by any particle. This component is called social knowledge. c_2 is the social factor which determines the extent of effect on the particle's direction by the gbest. The random numbers *rand*$_1$*()* and *rand*$_2$*()* provides a more random searchability to the PSO. Therefore, the three constants, *w*, c_1 and c_2 are instrumental in modifying the behaviour of the particles as the algorithm continues. In this paper, the cognitive and social factors are targeted to increase the performance of PSO [27].

In conventional swarm based optimisation, all the individual particles have similar behaviour in terms of local and global search. However, with better tuned cognitive and social leads, the algorithm attains a more randomised and direct search simultaneously. Hence, the different independent groups are utilised to update c_1 and c_2.

Using tuned coefficients of PSO has several advantages as compared to conventional PSO. Diverse patterns of c_1 and c_2 help to strike a balance between local and global search. Due to different updation strategies of c_1, local search space could be explored faster and more in a more randomised fashion than conventional PSO. Diverse updation strategies to update c_2 help to increase the social behavior of the particles.

Table 1 PSO coefficients updation

	Updation Equation	
Algorithm	C1	C2
Group 1	$(-2.05/T)t + 2.55$	$(1/T)t + 1.25$
Group 2	$(-2.05/T)t + 2.55$	$(2t^3/T)t + 0.5$
Group 3	$(-2t^3/T^3) + 2.5$	$(2t^3/T^3) + 1.25$
Group 4	$(-2t^3/T^3) + 2.5$	$(2t^3/T^3) + 1.25$

Initially, all the particles are clubbed randomly in different groups. At each iteration, fitness of the particles, gbest and pbest are stored. For each particle, the coefficients c_1 and c_2 are updated using the updation equations for different groups as shown in Table 1.

Using the new coefficients, velocity and position of particles are updated using (10) and (11).

This iterative procedure continues for each of the particles until the stopping criteria is met. Once, the stopping criteria is satisfied, the optimisation algorithm is exited. The flowchart for the modified PSO is presented in Figure 4.

4 Results and Discussions

The proposed system is tested for steady state conditions in grid connected mode of operation subject to constant solar irradiation. Moreover, the system is also subjected to dynamic conditions of change in irradiation, critical load control, mode transition from grid connected mode to islanded mode and vice-versa. Comparative performance of GA and modified PSO algorithms for DCVPI is also presented. The system complies with IEEE standards 1547 and 519.

4.1 Steady State Performance During Surplus PV Power Generation

Figure 5 describes the steady state performance of the system under constant irradiation (G) of 1000 W/m^2. PV array produces a power (P_{pv}) of 6.6 kW with PV voltage (V_{pv}) and PV current (I_{pv}) as depicted. The PV is meeting the load demand $(P_L)$of 3.2 kW and exporting power (P_g) of 2 kW to the grid. The surplus PV power is utilised in charging of EV. The negative sign of EV current (I_{EV}) follows from convention adopted for charging current. DC link voltage (V_{dc}) is regulated at 360V. Grid voltage (V_s) and current

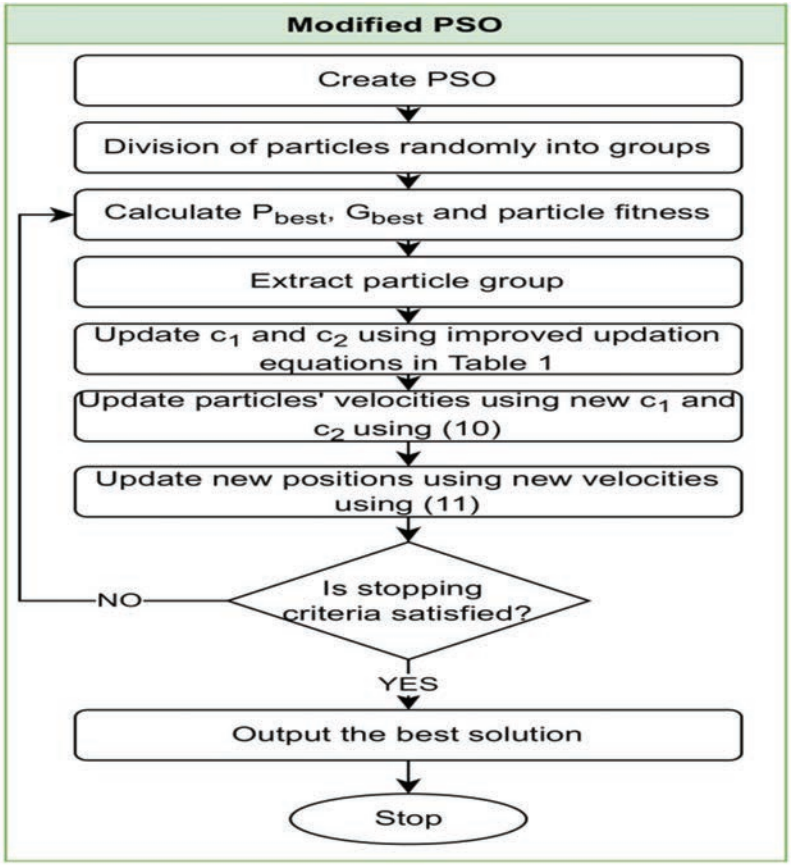

Figure 4 Flowchart depicting modified PSO.

(i_s) are in phase opposition denoting a power export and conform IEEE 519 standards of power quality.

4.2 Dynamic Performance of the System Under Insolation Fluctuation

Figure 6 presents the system performance under solar insolation fluctuation. Initially the system is exporting 2 kW to the grid and simultaneously meeting the load demand. At 0.4 s, solar irradiation (G) is reduced from 1000 W/m^2 to 600W/m^2. As a result, a dip in the PV current (I_{pv}) and PV array power (P_{pv}) is observed. Due to insufficient PV generation, EV begins to discharge

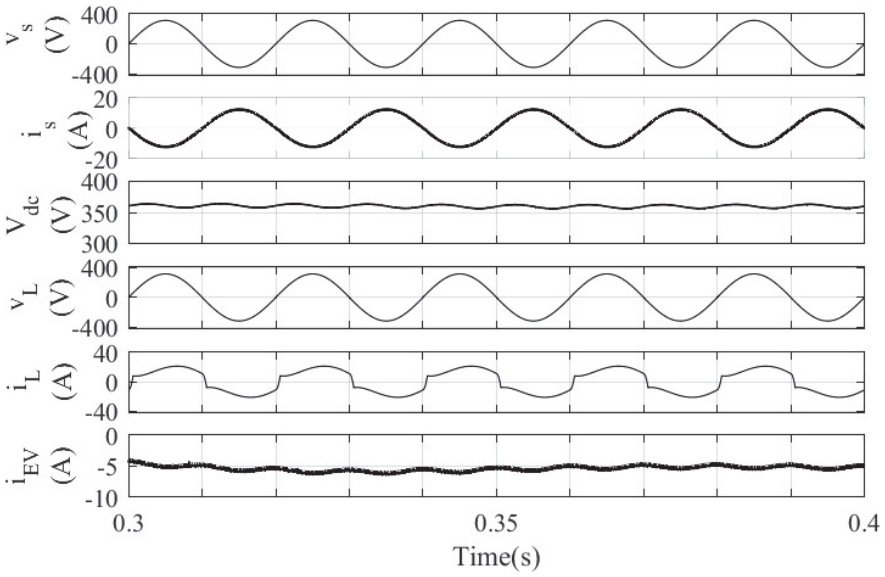

(a)

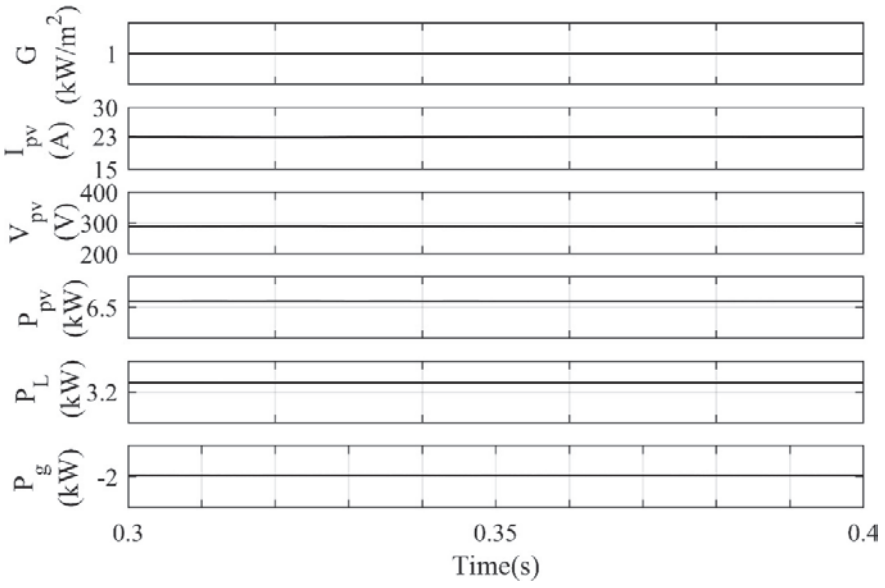

(b)

Figure 5 Steady state performance during surplus PV power mode at 1000W/m^2.

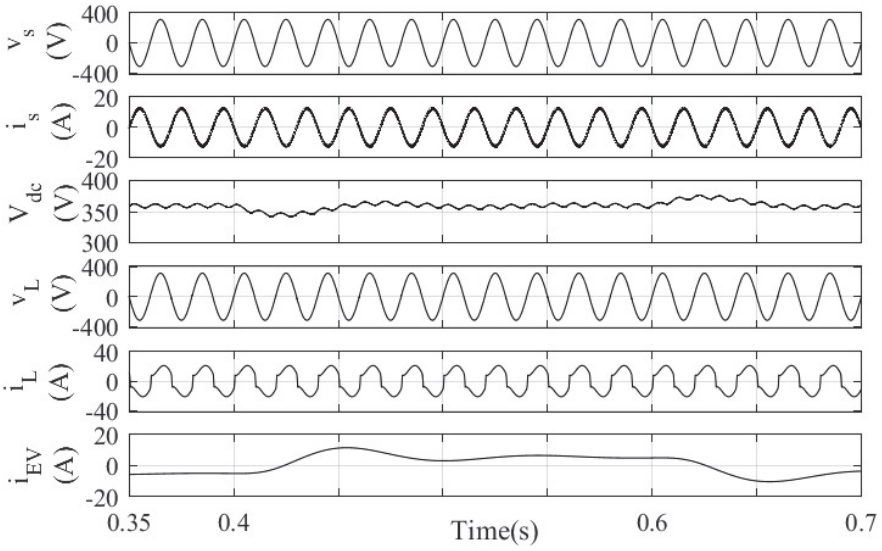

(a)

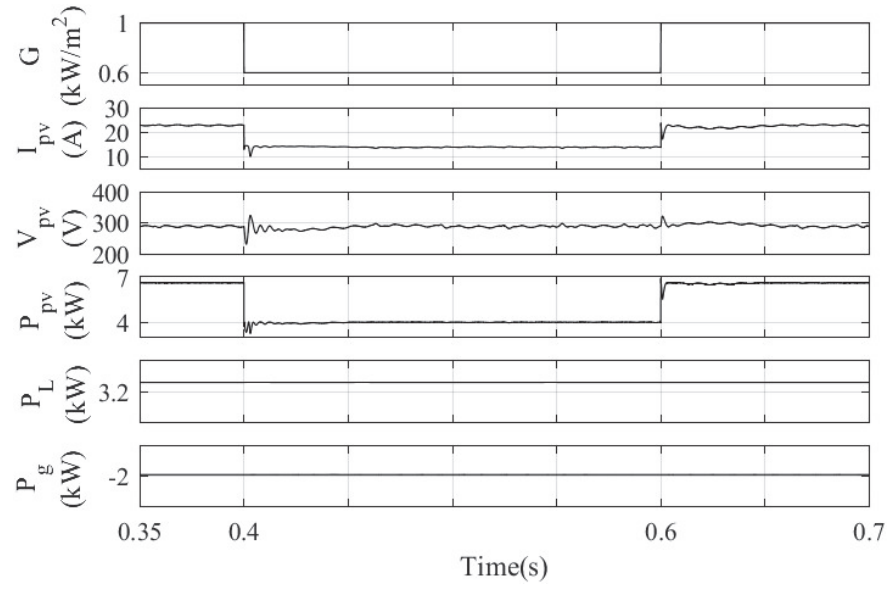

(b)

Figure 6 Dynamic performance of the system under solar insolation fluctuation.

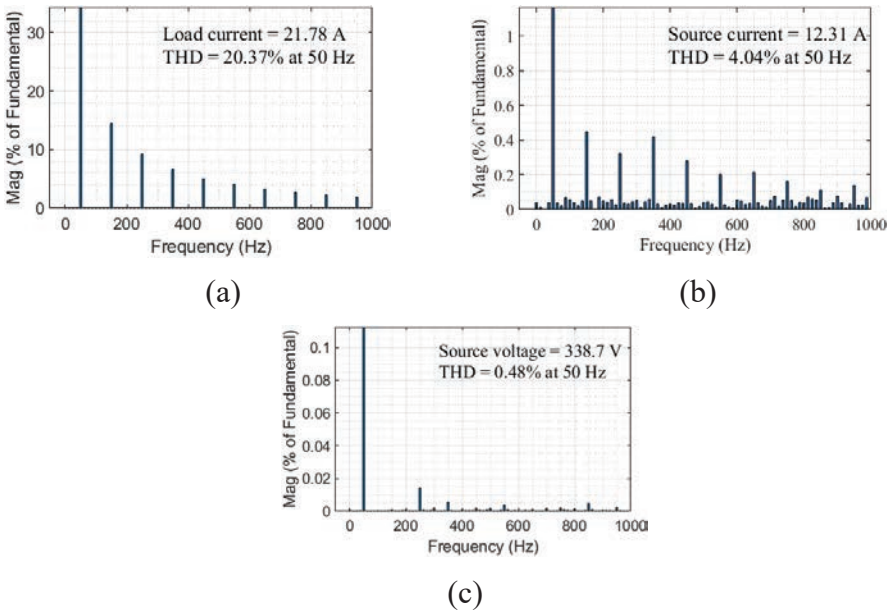

Figure 7 Harmonic content of (a) load current (b) Source current (c) Source voltage.

as observed by sign reversal of EV battery current (I_{EV}). At 0.6 s, irradiation again rises to 1000 W/m^2 and consequently EV begins to charge owing to sufficient PV output power. Other quantities remain unaffected by this operation. Harmonic spectrum of load current (i_L), grid voltage (V_s) and grid current (i_s) as depicted in Figure 7 demonstrates the compliance of the proposed system with IEEE power quality standard 519.

4.3 Dynamic Performance of the System Without PV Support Under Power Interruption with Priority Load Control

The system is tested for commonly occurring condition of power interruption in night hours when demand on the grid is highest. Initially, the grid is supplying 4 kW to the system, with load demand (P_L) of 3 kW. As depicted by Figure 8, the grid is disconnected at 0.7 s. Grid quantities (V_s), (i_s) and (P_g) are reduced to zero. The priority load control is activated and noncritical loads (P_L^{nCr}) are disconnected as observed by the load status, wherein '0' denotes disconnection and '1' symbolises connection. EV which was charging until now, now begins to discharge to provide power to the critical loads. When SOC of the battery reduces beyond 80%, the loads with

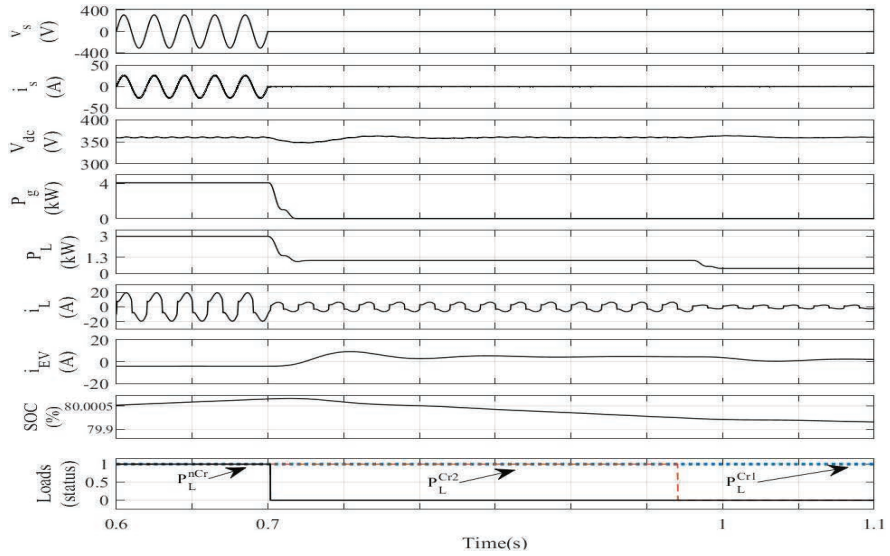

Figure 8 Dynamic performance of the system under power interruption with priority load control.

second priority are also disconnected, as demonstrated by waveforms of P_L and i_L. The results demonstrate the robustness of the control algorithm.

4.4 Dynamic Performance of the System Under Grid Resynchronisation Control

The performance of the proposed system is investigated for seamless resynchronisation with the grid once the fault is mitigated. As illustrated by Figure 9, the grid reappears at 0.5 s which is observed by the grid voltage (V_s) waveform. Resynchronisation controller comes into action and prevents the system from connecting to the grid as the phase error between load phase angle (θ_L) and grid phase angle (θ_s) is beyond the permissible limit as depicted in Figure 9. After 5 cycles, the synchronisation between system and grid is achieved and the system is brought on the grid as evident from grid current (i_g) and grid power (P_g) waveform. As demonstrated previously, priority load control reconnects the noncritical load after detecting presence of grid leading to increase in load power (P_L) and load current (i_L). Previously discharging EV also begins to charge evident from reversal of battery current (I_{EV}). The seamless mode switching from islanded mode to grid connected mode is ascertained.

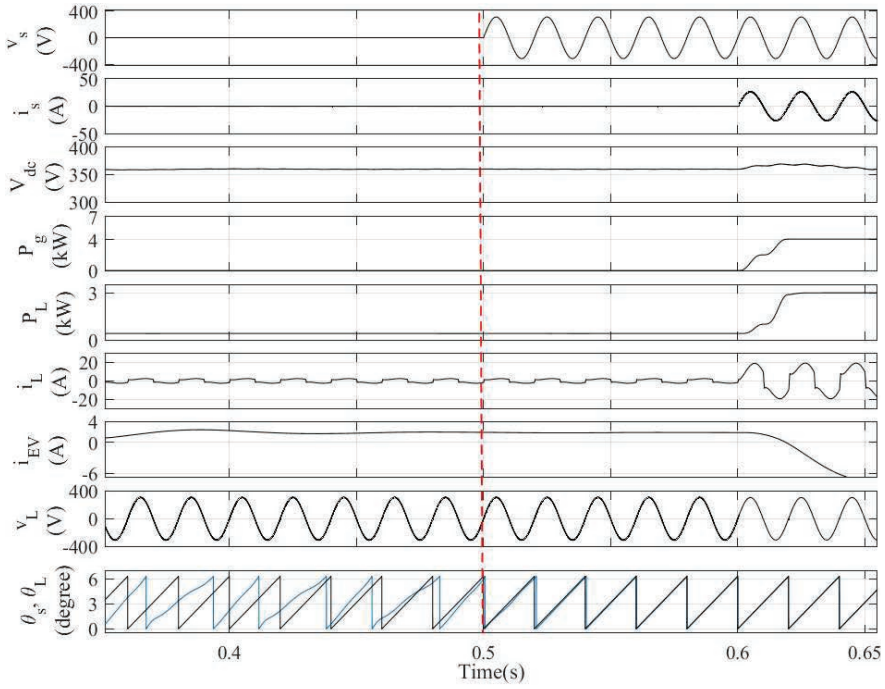

Figure 9 Dynamic performance of the system under grid resynchronisation control.

4.5 DC Link Optimisation Performance

The DCVPI gains are optimally tuned via modified PSO and GA algorithms for identical number of particles and iterations. Thus, in this article, DCVPI gains are tuned through modified PSO algorithm. Various dynamic conditions are simulated to evaluate the performance of the algorithms as depicted in Figure 10. Solar insolation G is varied from 1000 W/m^2 at 0.4 s to 600 W/m^2 at 0.6 s. Manually tuned DCVPI shows an dynamic state error of 4.44%, GA tuned gains depict an error of 4.7% whereas modified PSO tuned gains result in an error of 3.05% during the solar insolation. Similarly, solar insolation decrement results in 4.72% dynamic state error for manually tuned PI, 4.69% for GA tuned while only 3.05% for the modified PSO tuned. Moreover, load is perturbed from 0.65s to 0.75 s. The dynamic state error during load perturbation is 2.5% for the manually tuned PI, 2.77% for GA tuned PI whereas only 1.1% for modified PSO tuned DCVPI. In a similar fashion, a voltage sag from 220V to 175V is simulated at 0.8s, which results in 0.83% dynamic state error for manually tuned, 0.27% for GA tuned and 0.55% error

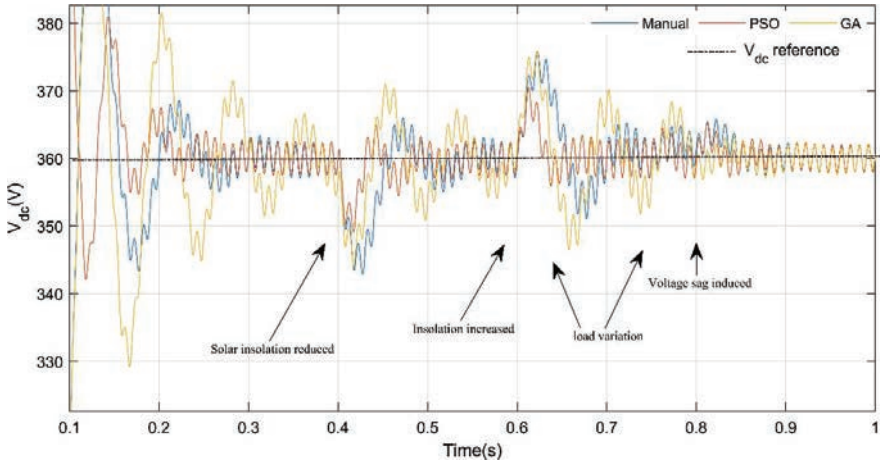

Figure 10 Comparative performance of algorithms for DC link PI tuning in presence of various dynamic conditions.

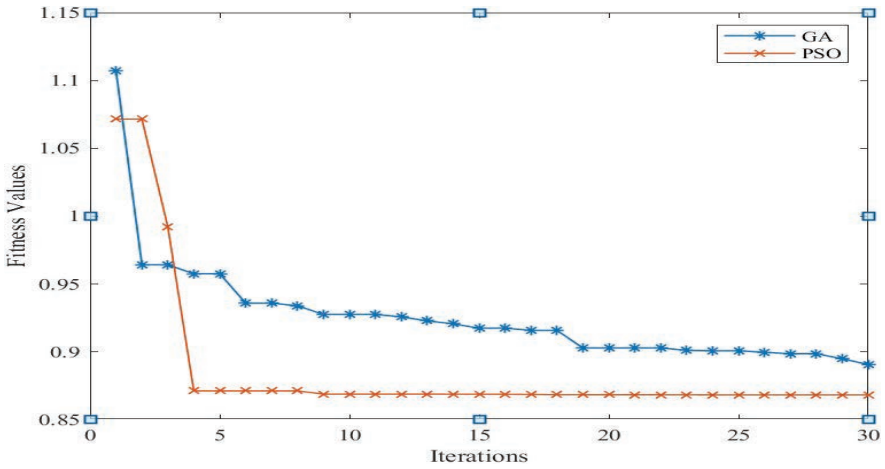

Figure 11 Convergence graph of fitness function evaluations for GA and PSO based tuning.

for modified PSO tuned system. The comparative fitness function evaluation for GA and modified PSO is shown in Figure 11. GA achieves a fitness function value of 0.89 in the 30th generation whereas modified PSO achieves a better fitness function value of 0.8684 in the 8th generation. Therefore, it is observed that modified PSO achieves faster convergence and better fitness function evaluation than GA. As evident from Figure 11, the optimally tuned

Table 2 Comparison of optimisation techniques

Algorithm	GA	Modified PSO
Objective function value attained	0.89	0.86
Number of iterations taken to reach minimum objective function value	30	8
Number of swarm particles	30	30
Range of k_{pv}	[0,20]	[0,20]
Range of k_{iv}	[0,50]	[0,50]

Table 3 DC link controller variables (k_{pv}, k_{iv})

Decision Variables	Without Optimisation	GA	Modified PSO
Proportional gain, k_{pv}	1	1.2	2.61
Integral gain, k_{iv}	22	49.97	50

Table 4 Comparative performance of optimised DC bus

Dynamic Conditions Created on the System	Manual	GA	Modified PSO
Computational burden	–	Moderate	Least
Dynamic-state error during solar insolation reduction	4.72%	4.69%	3.05%
Dynamic-state error during solar insolation increment	4.44%	4.7%	3.05%
Dynamic-state error during load perturbation	2.5%	2.77%	1.1%
Dynamic-state error during voltage sag	0.83%	0.27%	0.55%

gains using modified PSO result in less oscillations of the DC link voltage and it stabilises to the steady state value at a faster rate. The parameters of the optimisation algorithms are presented in Table 2. The values of the decision variables thus obtained are shown in Table 3. Modified PSO optimised DCVPI shows a better performance during the dynamic conditions as shown in Table 4.

5 Conclusion

In this article, a single phase solar powered grid tied residential premise with EV charging has been presented. A unique priority based critical loads selection algorithm has been implemented which selects the loads to be disconnected on the basis of the remaining SOC of the EV battery. This aids in extending the longevity of the EV battery by preventing excess stress on it. Various practical situations like variation in solar insolation, load variation and voltage sag and swells cause fluctuations in the DC link voltage. In order to regulate the DC link to its reference value, GA and modified

PSO algorithms have been implemented. It is observed modified PSO tuned gains result in faster convergence, better fitness function evaluation and superior system performance. Comparative performance of modified PSO and manually tuned PI has been presented for various dynamic conditions which indicates PSO tuned DCVPI produces an overshoot of 3.05% as opposed to 4.44% via manual tuning. Similarly, solar insolation decrement results in 4.72% dynamic state error for manually tuned PI, 4.69% for GA tuned while only 3.05% for the modified PSO tuned. The DC link voltage also stabilises to the reference voltage faster after experiencing a dynamic condition. Moreover, a seamless transition control between grid connected mode and islanded mode has been presented which depicts the robustness of the system. In case of islanded mode, EV battery supplies power to the loads.

Acknowledgement

The authors acknowledge the support provided by J&K Science and Technology & Innovation Council under the grant JKST&IC/75/2020.

Appendix

Boost Inductor, $L_b = 5$ mH, Bidirectional inductor, $L_{bt} = 7$ mH, AC inductor, $L_{ac} = 5$mH, RC Ripple Filter, $R_f = 5\Omega$ and $C_f = 15$ μF, DC Bus Voltage reference, $V_{ref} = 360$ V, EV battery (Lead Acid) Voltage = 240 V, EV battery capacity = 40 Ah.

References

[1] N. Saxena, I. Hussain, B. Singh, and A. L. Vyas, 'Implementation of a Grid-Integrated PV-Battery System for Residential and Electrical Vehicle Applications', *IEEE Trans. Ind. Electron.*, vol. 65, no. 8, pp. 6592–6601, Aug. 2018, doi: 10.1109/TIE.2017.2739712.

[2] R. M. Elavarasan *et al.*, 'A Comprehensive Review on Renewable Energy Development, Challenges, and Policies of Leading Indian States With an International Perspective', *IEEE Access*, vol. 8, pp. 74432–74457, 2020, doi: 10.1109/ACCESS.2020.2988011.

[3] C. Fang, H. Lu, Y. Hong, S. Liu, and J. Chang, 'Dynamic Pricing for Electric Vehicle Extreme Fast Charging', *IEEE Trans. Intell. Transp.*

Syst., vol. 22, no. 1, pp. 531–541, Jan. 2021, doi: 10.1109/TITS.2020.2983385.

[4] A. Verma and B. Singh, 'A Solar PV, BES, Grid and DG Set Based Hybrid Charging Station for Uninterruptible Charging at Minimized Charging Cost', 2018, p. 8.

[5] V. T. Tran, Md. R. Islam, K. M. Muttaqi, and D. Sutanto, 'An Efficient Energy Management Approach for a Solar-Powered EV Battery Charging Facility to Support Distribution Grids', *IEEE Trans. Ind. Appl.*, vol. 55, no. 6, pp. 6517–6526, Nov. 2019, doi: 10.1109/TIA.2019.2940923.

[6] Q. Yan, B. Zhang, and M. Kezunovic, 'Optimized Operational Cost Reduction for an EV Charging Station Integrated With Battery Energy Storage and PV Generation', *IEEE Trans. Smart Grid*, vol. 10, no. 2, pp. 2096–2106, Mar. 2019, doi: 10.1109/TSG.2017.2788440.

[7] S. Chauhan and B. Singh, 'Control of solar PV-integrated battery energy storage system for rural area application', *IET Renew. Power Gener.*, vol. 15, no. 5, pp. 1030–1045, Apr. 2021, doi: 10.1049/rpg2.12086.

[8] T. Ma and O. A. Mohammed, 'Optimal Charging of Plug-in Electric Vehicles for a Car-Park Infrastructure', *IEEE Trans. Ind. Appl.*, vol. 50, no. 4, pp. 2323–2330, Jul. 2014, doi: 10.1109/TIA.2013.2296620.

[9] Y. Wu, J. Zhang, A. Ravey, D. Chrenko, and A. Miraoui, 'Real-time energy management of photovoltaic-assisted electric vehicle charging station by markov decision process', *J. Power Sources*, vol. 476, p. 228504, Nov. 2020, doi: 10.1016/j.jpowsour.2020.228504.

[10] F. Giordano et al., 'Vehicle-to-Home Usage Scenarios for Self-Consumption Improvement of a Residential Prosumer With Photovoltaic Roof', *IEEE Trans. Ind. Appl.*, vol. 56, no. 3, pp. 2945–2956, May 2020, doi: 10.1109/TIA.2020.2978047.

[11] X. Ran and K. Liu, 'Robust Scatter Index Method for the Appliances Scheduling of Home Energy Local Network With User Behavior Uncertainty', *IEEE Trans. Ind. Inform.*, vol. 15, no. 7, pp. 4129–4139, Jul. 2019, doi: 10.1109/TII.2019.2897126.

[12] A. Alsabbagh, B. Wu, and C. Ma, 'Distributed Electric Vehicles Charging Management Considering Time Anxiety and Customer Behaviors', *IEEE Trans. Ind. Inform.*, vol. 17, no. 4, pp. 2422–2431, Apr. 2021, doi: 10.1109/TII.2020.3003669.

[13] M. Chankaya, I. Hussain, and A. Ahmad, 'Seamless control of grid-tied PV-Hybrid Energy Storage System', *Int. J. Emerg. Electr. Power Syst.*,

vol. 0, no. 0, p. 000010151520210090, Jun. 2021, doi: 10.1515/ijeeps-2021-0090.

[14] M. Ganjian-Aboukheili, M. Shahabi, Q. Shafiee, and J. M. Guerrero, 'Seamless Transition of Microgrids Operation From Grid-Connected to Islanded Mode', *IEEE Trans. Smart Grid*, vol. 11, no. 3, pp. 2106–2114, May 2020, doi: 10.1109/TSG.2019.2947651.

[15] S. Taghizadeh, M. J. Hossain, J. Lu, and M. Karimi-Ghartemani, 'An Enhanced DC-Bus Voltage-Control Loop for Single-Phase Grid-Connected DC/AC Converters', *IEEE Trans. Power Electron.*, vol. 34, no. 6, pp. 5819–5829, Jun. 2019, doi: 10.1109/TPEL.2018.2866501.

[16] L. F. Alves Pereira and A. Sanfelice Bazanella, 'Tuning Rules for Proportional Resonant Controllers', *IEEE Trans. Control Syst. Technol.*, vol. 23, no. 5, pp. 2010–2017, Sep. 2015, doi: 10.1109/TCST.2015.2389655.

[17] N. Babu P, J. M. Guerrero, P. Siano, R. Peesapati, and G. Panda, 'An Improved Adaptive Control Strategy in Grid-Tied PV System With Active Power Filter for Power Quality Enhancement', *IEEE Syst. J.*, vol. 15, no. 2, pp. 2859–2870, Jun. 2021, doi: 10.1109/JSYST.2020.2985164.

[18] S. Kakkar et al., 'Design and Control of Grid Connected PWM Rectifiers by Optimizing Fractional Order PI Controller using Water Cycle Algorithm', *IEEE Access*, pp. 1–1, 2021, doi: 10.1109/ACCESS.2021.3110431.

[19] T. A. Naidu, S. R. Arya, R. Maurya, B. Singh, and A. Al-Durra, 'Combined Variable Step Size LMS for DVR with Error Regulator Gain Tuning Through Ant-Lion Optimization', in *2020 IEEE Industry Applications Society Annual Meeting*, 2020, pp. 1–8. doi: 10.1109/IAS44978.2020.9334758.

[20] F. A. Alturki, H. O. Omotoso, A. A. Al-Shamma'a, H. M. H. Farh, and K. Alsharabi, 'Novel Manta Rays Foraging Optimization Algorithm Based Optimal Control for Grid-Connected PV Energy System', *IEEE Access*, vol. 8, pp. 187276–187290, 2020, doi: 10.1109/ACCESS.2020.3030874.

[21] A. Alhejji and M. I. Mosaad, 'Performance enhancement of grid-connected PV systems using adaptive reference PI controller', *Ain Shams Eng. J.*, vol. 12, no. 1, pp. 541–554, Mar. 2021, doi: 10.1016/j.asej.2020.08.006.

[22] K. Premkumar, M. Vishnupriya, T. Thamizhselvan, P. Sanjeevikumar, and B. V. Manikandan, 'PSO optimized PI controlled DC-DC buck

converter-based proton-exchange membrane fuel cell emulator for testing of MPPT algorithm and battery charger controller', *Int. Trans. Electr. Energy Syst.*, vol. 31, no. 2, Feb. 2021, doi: 10.1002/2050-7038.12754.

[23] S. Pradhan, I. Hussain, B. Singh, and B. Ketan Panigrahi, 'Performance Improvement of Grid-Integrated Solar PV System Using DNLMS Control Algorithm', *IEEE Trans. Ind. Appl.*, vol. 55, no. 1, pp. 78–91, Jan. 2019, doi: 10.1109/TIA.2018.2863652.

[24] R. B. Roy et al., 'A Comparative Performance Analysis of ANN Algorithms for MPPT Energy Harvesting in Solar PV System', *IEEE Access*, vol. 9, pp. 102137–102152, 2021, doi: 10.1109/ACCESS.2021.3096864.

[25] N. Kumar, I. Hussain, B. Singh, and B. K. Panigrahi, 'Rapid MPPT for Uniformly and Partial Shaded PV System by Using JayaDE Algorithm in Highly Fluctuating Atmospheric Conditions', *IEEE Trans. Ind. Inform.*, vol. 13, no. 5, pp. 2406–2416, Oct. 2017, doi: 10.1109/TII.2017.2700327.

[26] S. Deo, C. Jain, and B. Singh, 'A PLL-Less Scheme for Single-Phase Grid Interfaced Load Compensating Solar PV Generation System', *IEEE Trans. Ind. Inform.*, vol. 11, no. 3, pp. 692–699, Jun. 2015, doi: 10.1109/TII.2015.2425138.

[27] S. Mirjalili, A. Lewis, and A. S. Sadiq, 'Autonomous Particles Groups for Particle Swarm Optimization', *Arab. J. Sci. Eng.*, vol. 39, no. 6, pp. 4683–4697, Jun. 2014, doi: 10.1007/s13369-014-1156-x.

Biographies

Masiha Aijaz received the B.Tech. degree in electrical engineering from Islamic University of Science & Technology, Jammu & Kashmir, India in 2016 and the M.Tech. degree in electrical engineering from Jamia Millia Islamia, New Delhi, India in 2018. She is currently working toward the Ph.D. degree in electrical engineering with the Department of Electrical Engineering, National Institute of Technology Srinagar, India. Her research interests include power quality improvement in distribution networks, renewable energy based electric vehicle charging and adoption of optimisation algorithms in electric vehicle charging applications.

Ikhlaq Hussain received his B. E. (Electrical) from University of Jammu, Jammu, India, in 2009, M. Tech. (Gold Medallist) in Electrical Power System Management from the Jamia Millia Islamia (A Central University), New Delhi, India, in 2012 and PhD in the Department of Electrical Engineering, Indian Institute of Technology Delhi, New Delhi, India, in 2018. Since 2018, he has been working as an assistant professor in the department of electrical engineering in University of Kashmir, Jammu and Kashmir, India.

His areas of research interests include power electronics, power quality, custom power devices, renewable energy systems, optimisation algorithms, electric vehicle charging and microgrid. Dr. Hussain was a recipient of the POSOCO power system award (PPSA), Gandhian Young Innovations Award in 2018, Outstanding Faculty researcher in the field of energy for 2017–2018. He has participated as a young scientist in 3rd BRICS young scientist conclave from 25th to 29th June 2018 at Durban, South Africa by department of Science & technology, Govt. of India. He has filed 7 patents and awarded 1 national patent. He has coauthored more than 60 IEEE transactions and 100 conference papers. He has been featured twice in the Stanford list of world's top 2% researchers in the field of energy.

Shameem Ahmad Lone received his M.E. (Gold Medallist) in 1998 from Indian Institute of Technology, Roorkee, India and Ph.D. in Electrical Engineering in 2007 from National Institute of Technology, Srinagar, India. Since 1994, he has been working in department of Electrical Engineering, National Institute of Technology Srinagar, where currently he is a senior professor. His research interests include stand-alone power systems, hybrid and weak power systems, role of energy storage in improving the power quality, intelligent control techniques. He has published several research papers in reputed national and international journals, and conference proceedings.